AERE— R-7318

United Kingdom Atomic Energy Authority

RESEARCH GROUP

Report

THE DEVELOPMENT OF ENHANCED HEAT TRANSFER CONDENSER TUBING

I. H. NEWSON T. D. HODGSON

Chemical Engineering and
Process Technology Divisions,
Atomic Energy Research Establishment,
Harwell, Berkshire.

1973

With Compliments

OFFICE OF NAVAL RESEARCH, BRANCH OFFICE
Box 39
Fleet Post Office New York 09510

THE DEVELOPMENT OF ENHANCED HEAT TRANSFER CONDENSER TUBING

by

I. H. Newson* and T. D. Hodgson+

ABSTRACT

Methods for manufacturing a variety of shapes of enhanced heat transfer condenser tubing have been developed. 32 different tubes have been studied, in a vertical orientation, for their overall heat transfer and pressure drop characteristics. All experiments were conducted with atmospheric steam condensing on the outside of the tube and water in forced convective flow on the inside, the heated length of the tube being 45 ins. (114 cm). The results show that on the condensing steam side coefficients up to 6 times comparable smooth tube values were obtained, and on the forced convective side up to 2½ times. The results are linked to tube shape and appropriate theoretical analyses are presented.

*Chemical Engineering Division,
+Process Technology Division,
U.K.A.E.A. Research Group,
Atomic Energy Research Establishment,
HARWELL

July 1973

/PS

HL73/2805(C6)

CONTENTS

TABLES

ILLUSTRATIONS

1. Introduction

There is a growing interest in the use of enhanced heat transfer tubing in all forms of sea water evaporation plants. Most of the research effort so far appears to have been devoted to the development of an enhanced fluted tube suitable for use in the falling film mode in the multiple effect (ME) evaporator system[1,2]. The benefits of this type of tube in reducing water costs from ME plants (as shown by design studies) is by now well known. The U.K.A.E.A. has over the last few years developed commercially practical methods of manufacturing enhanced heat transfer tubing of several different types. These types are suitable for ME plants, as mentioned above, and also for advanced designs of multistage flash (MSF) plants.

This paper describes the types of enhanced condenser tubing which have been developed and studied at the Harwell Research Establishment. These tubes were specifically designed for use in advanced MSF plants, but they could also find use in the preheaters of a ME train. The heat transfer and pressure drop characteristics of the several different types of tubing are presented and indications given of how they could be most efficiently used.

2. Types of Enhanced Heat Transfer Condenser Tubing

Figure 1 shows general and cross section views of six different types of tubing which span the range of development. All tubes shown were constructed from tubing initially of 1¼ in. (31.8 mm) outside diameter (O.D.). Referring to Figure 1 the several types can be identified as follows:

(a) 4 start, swaged (or "roped") helical,
(b) 4 start, positive indentation helical,
(c) 8 start, swaged helical,
(d) 8 start, longitudinal wave,
(e) 16 start, multifluted,
(f) 30 start, multifluted, high density fluting.

Type (a), the swaged or "roped" type of tubing is probably the best known and has been the subject of previous studies[3,4]. Type (b), while similar to type (a), was, nevertheless, constructed in such a manner as to produce more positive curvatures surrounding the indentations as shown in the cross section views. This feature is reflected in the tube performance. Type (c), the 8 start swaged tube, is similar to type (a) but, for any chosen angle of indentation, provides twice as many indentations per unit length of tube.

The longitudinal wave tube, type (d), was developed to contrast specifically with the tube side characteristics of the previous three types. With fluid flowing inside the tubes, types (a), (b) and (c) tend to induce a swirling flow pattern while increasing the heat transfer rate. Theoretical analysis of this type of flow indicated that the increased friction loss must always be much greater than the increased heat transfer rate. The longitudinal wave profile therefore was designed to increase the heat transfer rate while avoiding the swirl flow mechanism.

Types (e) and (f), the multifluted tubing, appear radically different to the foregoing types. The method of construction differs also, and one can see that greater deformation of the original smooth tube occurs. Because of this greater metal deformation and

especially to prevent appreciable localised thinning of the tube wall, the helix leads H (for definition see below) are generally longer than for the swaged type of tube. This limitation has its effect on the heat transfer and pressure drop characteristics of this type of tube.

Some relevant definitions relating to profiled tubing of the above types are given below:

Helix Lead H = Distance along tube axis taken by an indentation in turning through 360^0

Helix Ratio H_R = $\frac{\text{Helix Lead, H}}{\text{Tube inside perimeter, } P_i}$

Indentation Ratio δ = $\frac{\text{Indentation depth, e}}{\text{Hydraulic Diameter, } D_h}$

Hydraulic Diameter D_h = $\frac{4 \times \text{cross sectional area, } A_i}{\text{Tube inside perimeter, } P_i}$

Altogether 17 tubes of types (a) and (b), 7 tubes of types (c) and (d) and 8 tubes of types (e) and (f) were studied in the series of experiments discussed in this paper. Tables 1, 2 and 3 give details of the important dimensions of the three groups of tubes. The theoretical analyses presented in this paper have been applied only to tubes of types (a), (b) and (c). Detailed performance analysis of tubes of types (d), (e) and (f) are not given here, and for these tubes only general performance data are quoted.

Table 1

Physical Dimensions of 4 Start Tubes (Types (a) and (b)) used for Experiments

Tube Number	Tube Type	Number of Starts	Helix Ratio (H_R)	Indentation Ratio (δ)	Hydraulic Diameter (D_h)
S. 3	(a)	4	0.674	0.0775	1.122
S. 12	(a)	4	1.052	0.0487	1.160
S. 13	(a)	4	1.750	0.0626	1.158
S. 14	(a)	4	2.52	0.0634	1.142
S. 17	(a)	4	0.477	0.0667	1.072
S. 18	(a)	4	0.958	0.1056	1.057
S. 19	(a)	4	1.60	0.1127	1.039
S. 20	(a)	4	2.55	0.1087	1.050
S. 21	(a)	4	0.210	0.0228	1.093
S. 22	(a)	4	0.280	0.0272	1.102
S. 37	(a)	4	2.68	0.0618	1.122
S. 43	(a)	4	0.608	0.0271	1.182
S. 44	(a)	4	0.656	0.0520	1.120
S. 46	(a)	4	0.670	0.1140	1.000
RM 40	(b)	4	2.14	0.1138	0.990
RM 41	(b)	4	1.36	0.0883	1.030
R 42	(a)	4	0.750	0.0872	1.068

Table 2

Physical Dimensions of 8 Start Tubes
(Types (c) and (d)) used for Experiments

Tube Number	Tube Type	Number of Starts	Helix Ratio (H_R)	Indentation Ratio (δ)	Hydraulic Diameter (D_h)
S. 4	(c)	8	1.00	0.0500	0.936
S. 7	(c)	8	0.732	0.0347	0.994
S. 9	(c)	8	0.677	0.0328	1.025
S. 10	(c)	8	1.972	0.0557	1.015
S. 11	(c)	8	2.732	0.0548	1.032
S. 16	(c)	8	1.560	0.0462	1.050
S. 8	(d)	8	-	0.0707	0.986

Table 3

Physical Dimensions of Multifluted Tubes
(Types (e) and (f)) used for Experiments

Tube Number	Tube Type	Number of Starts	Helix Ratio (H_R)	Indentation Ratio (δ)	Hydraulic Diameter (D_h)
G. 6	(e)	16	2.065	0.0492	0.936
G. 30	(e)	16	1.987	0.0625	0.934
G. 31	(e)	16	2.552	0.0695	0.919
G. 32	(e)	16	1.356	0.0531	1.026
G. 33	(e)	16	4.145	0.0506	0.949
G. 35	(e)	20	2.558	0.0477	0.922
G. 36	(e)	20	2.463	0.0581	0.900
G. 47	(f)	30	3.995	0.0470	0.8995

3. Apparatus and Experimental Procedure

The purpose of the initial experimental work presented here was to examine a large number of different tube shapes, and from the results to link tube performance with characteristic shape parameters. For this tube screening exercise, therefore, all experiments were conducted with steam at atmospheric pressure condensing on the outside of a vertically mounted profiled condenser tube, with water in forced convective (non-boiling) flow being pumped through the tube. The heated length of tube in each case was 45 ins. (1.14 m), and the logarithmic mean temperature difference (LMTD) for the experiments was maintained at 11°F (6.1°C).

Measurements of overall heat transfer coefficient U and pressure drop ΔP, over the tube length, were obtained. From the measured values of U, the condensing side coefficient

h_o and water side coefficient h_i were calculated using a more comprehensive version of the Wilson plot technique[5]. The theoretical analyses were aimed primarily at interpreting and correlating the h_i and pressure drop results. The pressure drop measurements were extended to much lower Reynolds Numbers than occurred under the heat transfer conditions by repeating these runs under isothermal, cold flow (70°F, 21°C) conditions. The experimental apparatus is show schematically on Figure 2.

The enhanced tube under test was held at each end within resin blocks of non-conducting material. The smooth sections left at each end of the enhanced tube fitted snugly inside "O" rings let into grooves in the resin blocks. As shown in Figure 2 the resin blocks and tube were contained within a glass steam jacket which was fed with steam taken from the mains supply. Deflecting baffles were placed to prevent direct impingement of the steam on the tube under test, as this would have generated spurious heat transfer results. The condensate forming on the tube was collected in a cup cast into the resin block at the bottom of the tube, and its rate of flow was periodically measured to obtain a heat balance. The heat balances usually showed heat losses of about 5 to 10%. The steam pressure in the jacket was kept a few cms water gauge above atmospheric pressure. This ensured a steady vented flow of steam to atmosphere to avoid accumulation of non-condensible gases. The saturated steam temperature, T_v, used for calculations was computed from the steam manometer and absolute pressure. Great care was taken, by means of an established tube cleaning and wetting sequence, to avoid the occurrence of unpredictable dropwise condensation on the tube.

The water circuit was a closed recirculating system around which demineralised water was pumped, the rate of water flow through the tube being determined by direct weighing over a timed interval. Just before entry to the test section the water flowed through a 2 ft (0.61 m) length of tube of the same profile as that under test. Pressure drop measurements were made by means of pressure tappings let into the resin sections, see Figure 2, and recorded on a vertical water manometer. The pressure drop measured was that over the 45 in. (1.14 m) length of profiled tube section, plus two lengths of smooth tubing left at either end of the tube for sealing, plus two short lengths of smoothly bored resin blocks. A procedure was adopted which effectively subtracted the contribution of the end pieces leaving only the pressure drop over the profiled section.

Accurate determination of the important tube dimensions is vital for meaningful interpretation of each tube's performance. The important dimensions are the helix lead, the cross sectional area for flow, the inside and outside perimeters and the average wall thickness.

The cross section area for flow was found by determining the weight of water to fill the profiled length of tube. Perimeters were found by measurement from photographs (magnified five times) of samples of profiled cross sections. Typical photographs of cross sections are shown on Figure 1. The average wall thickness was found from volume displacement of water and the average of outside and inside perimeters. The depth of profile indentation was determined by micrometer measurements on the tube itself. The results of this type of tube characterisation are included in Tables 1, 2 and 3.

4. Theoretical Analysis - Tube Types (a), (b) and (c)

The heat transfer and pressure drop obtained during water flow in the profiled tubes is analysed in terms of a Swirl Flow theory. This theory attempts to predict the increase of heat transfer rate and friction factor over smooth tube values for the same operating conditions. A simple model has also been derived to predict the condensing side coefficient on the vertical roped and indented surfaces.

4.1 Swirl Flow Model - Tube Side Heat Transfer Analysis

The model assumes that the fluid flowing within the tube follows exactly the spiral path of the indentations which are assumed to lie at an angle θ (see Figure 3) to the axis of the tube. (The criteria to make the fluid swirl are not considered here.) Details of the analysis are given in the Appendix. The analysis makes use of the Dittus - Boelter[6] equation for the tube side heat transfer coefficient, h_s, in a smooth tube

$$\frac{h_s D_s}{k} = \varepsilon_s \left(\frac{\rho V_s D_s}{\mu}\right)^{0.8} Pr^{0.4} \qquad (1)$$

and gives for h_r in the profiled tube

$$\frac{h_r}{h_s} = \left(1 + \frac{1}{H_R^2}\right)^{0.4} = \frac{\varepsilon_r}{\varepsilon_s} \qquad (2)$$

provided the profiling does not significantly change the hydraulic diameter of the smooth tube (the coefficients h_r and h_s only vary as $D^{-0.2}$).

The analysis relates the heat transfer ratio (h_r/h_s) simply to the helix ratio H_R i.e. to the angle of the indentation.

4.2 Swirl Flow Model - Tube Side Pressure Drop Analysis

The analysis of the tube side pressure drop in the profiled tube ΔP_r is based on analogy with the well known[7] equation for the pressure drop, ΔP_s, in a smooth tube, given by

$$\Delta P_s = 8 f_s \frac{L}{D_s} \frac{V_s^2}{2g} \qquad (3)$$

Details of the swirl flow analysis are given in the Appendix. The analysis expresses the friction factor ratio (f_r/f_s) between profiled and smooth tubes in terms of the helix ratio H_R

$$\frac{f_r}{f_s} = \left(1 + \frac{1}{H_R^2}\right)^{1.38} \qquad (4)$$

4.3 Comparison of Heat Transfer and Friction Factor Enhancement

Equations (2) and (4) express the magnitudes of the increases to be expected in the heat transfer coefficients and friction factors as a result of profiling. If the analogy between heat and momentum transfer were to hold, an increase in heat transfer would be matched by an equivalent increase in friction factor. In fact equations (2)

and (4) indicate that this analogy cannot be expected to hold for this type of tubing. Thus, as the helix ratio decreases, the friction factor ratio increases faster than the heat transfer ratio.

It is convenient to define a Performance Ratio, γ, where

$$\gamma = \frac{h_r/h_s}{f_r/f_s} = \frac{1}{(1 + 1/H_R^2)^{.98}} \triangleq \frac{1}{(1 + 1/H_R^2)}$$

The performance ratio clearly decreases as the helix ratio increases. For a value of $H_R = 1$, which is about the middle of the range of practical interest, $\gamma = 0.5$. The value of γ is equal to 1 only for the smooth tube case, and one might infer therefore that the smooth tube is always more "efficient" than a profiled one. However it can still be worthwhile to use a profiled tube instead of a smooth one, since the economic case depends on several other criteria besides the above.

4.4 Prediction of Condensing Side Coefficient for Vertical Profiled Tubes

The model on which the condensing side analysis is based assumes that the indentations on the outside of the tube effectively reduce the drainage height for the condensate film to the distance (l) between successive indentations (see Figure 3). This follows from assuming that each indentation holds, by means of surface tension forces, all the condensate that drains into it, and prevents the continuous build-up of the condensate film over the whole length of the vertical tube. The drainage is therefore mostly carried by the indentations. The model further assumes that, because of the thickness of the condensate layer in these indentations, the area of the indentations plays no part in the actual condensation process. Hence, because of the reduced drainage height, the average film thickness between successive indendations is decreased and the overall condensing coefficient is increased over smooth tube values.

Note that surface tension acts to channel condensate drainage in the above model and therefore the model is applicable only to tubes in the groups (a), (b) and (c) of Figure 1. For tubes of types (e) and (f) surface tension forces on the particular tube shapes act to <u>increase</u> drainage and by this means enhance the condensing side coefficient.

The profiled tube condensing coefficient h_o' is derived by analogy with the Nusselt[8] equation for the average condensing coefficient h_o over a length L of vertically disposed smooth tube with zero film thickness at the top. This equation is

$$h_o = 0.925 \left[\frac{\rho^2 g \lambda k^3}{\mu} \cdot \frac{A_o}{LQ} \right]^{1/3} \qquad (5)$$

$$\text{or} \qquad h_o = 0.925 \left[K \frac{A_o}{LQ} \right]^{1/3}$$

where K represents the contribution of the physical properties of the condensed fluid.

Details of the derivation of h_o' are given in the Appendix but the analysis yields

$$\frac{h_o'}{h_o} = \left(\frac{H - Nb}{H}\right)\left(\frac{L}{H/N - b}\right)^{\frac{1}{4}} \qquad (6)$$

where the profiled (h_o') and smooth tube (h_o) average condensing coefficients are compared for assumed identical temperature driving force conditions ΔT_o.

Equation (6) expresses the enhancement of the condensing side coefficient to be expected with the profiled tube in terms of the tube profile geometry (see Figure 3). Once the length of vertical tube, L, has been fixed for experimental purposes, values of the enhancement can be calculated from equation (6) by assigning typical values of helix lead H, number of starts N and width of groove b. With typical values of L and b taken as 45 in. (1.14 m) and 0.1 in. (2.54 mm) respectively, and with helix lead as a variable, calculations show that the maximum enhancement possible is about 3. This occurs at a helix lead of about 1.2 in. (30.5 mm) for the 4 start tubes and 2.4 in. (61 mm) for the 8 start tubes.

5. Experimental Results

The experimental measurements are presented under separate headings of heat transfer and pressure drop.

5.1 Heat Transfer Measurements

Figures 4, 5 and 6 show, for selected tubes, values of measured overall heat transfer coefficients U_o (based on the tube outer surface area A_o) plotted against the water velocity V_s into the tube smooth end. Curves of smooth tube performance are also shown for comparison, and on the above basis comparison is made between smooth and profiled tubes handling the same mass flow of fluid. The average water side temperature was about 200°F (93°C) for all experiments and the logarithmic mean temperature difference (LMTD) was about 11°F (6°C). The plots show that for the 4 and 8 start type of swaged tube the helix ratio H_R provides the dominant effect upon the value U_o, which increases with decreasing values of H_R.

From curves such as on Figures 4, 5 and 6 the values of the condensing steam side coefficient h_o and water side coefficient h_i were derived using the Wilson plot technique as outlined below. The overall heat transfer coefficient U_o is related to the individual coefficients by the well known equation

$$\frac{1}{U_o} = \frac{1}{h_o} + \frac{x_w}{k_w}\frac{A_o}{A_w} + \frac{1}{h_i}\frac{A_o}{A_i} \qquad (7)$$

where subscripts o and i refer to tube outer and inner surfaces respectively. The water side forced convective coefficient h_i can be expressed using a recent correlation[9]. For smooth tubes

$$\frac{h_i D}{k} = \varepsilon_s \, Re^{0.795} \, Pr^{y} \qquad (8)$$

where the exponent y on the Prandtl Number Pr ($= \frac{C\mu}{k}$) is given by

$$y = 0.495 - 0.0025 \ln Pr$$

For a smooth tube the value $\varepsilon_s = 0.0225$. Combining all the physical property terms in equation (8) into a single term Ω we have the analogous equation for the profiled tube

$$h_i = \varepsilon_r \, \Omega \, V^{0.795} \tag{9}$$

The condensing side coefficient h_o can be expressed as in equation (5), based on Nusselt's derivation

$$h_o = \beta \left(\frac{\rho^2 g \lambda k^3}{\mu} \cdot \frac{A_o}{LQ} \right)^{1/3} = \beta (\nu)^{1/3} \tag{10}$$

It is assumed that this equation is valid for the 4 and 8 start swaged tubes since condensation should be more nearly laminar because of the greatly reduced drainage lengths. β is a constant depending on the tube profile and for a smooth tube is, theoretically, equal to 0.925.

Substituting for h_i and h_o equation (7) becomes

$$\nu^{1/3} \left(\frac{1}{U_o} - \frac{x_w}{k_w} \frac{A_o}{A_w} \right) = \frac{1}{\beta} + \frac{1}{\varepsilon} \left(\frac{A_o \, \nu^{1/3}}{A_i \, \Omega \, V^{0.795}} \right) \tag{11}$$

or

$$Y = \frac{1}{\beta} + \frac{1}{\varepsilon} X$$

Hence a plot of Y and X should give a straight line of slope $\frac{1}{\varepsilon}$ and intercept $\frac{1}{\beta}$. The individual coefficients h_i and h_o can then be calculated from equations (8) and (10) respectively. The above form of the Wilson plot takes account of the variation of the condensing side coefficient h_o with heat flux Q, which for these experiments was effectively determined by the water side velocity V.

For each tube the measured set of data points Y and X was fitted with a best straight line assuming a regression of the heat transfer term Y on the "velocity" term X. Good straight lines were obtained for each set of data points, thus justifying the assumptions inherent in the above derivations. For the smooth tube, values of ε_s and β were obtained for both brass and copper tubes. These values were respectively, 0.0226, 1.230 and 0.0226, 1.452. These may be compared with the established values 0.0? 5 and 0.925. The condensing coefficient value $\beta_s = 0.925$ was derived by Nusselt for laminar flow conditions. It is well known that under turbulent film flow with waves forming on the condensate film, as was observed here, values in excess of 0.925 will occur. For example, an analysis by Dukler[10] allowing for the effect of turbulence, but not wave flow, gave $\beta_s = 1.42$ for condensate loadings comparable to those in this work.

Figures 7 to 10 show values of h_i and h_o derived from the above analysis for some of the 4 and 8 start swaged tubes and the multifluted tubes. The intercept of the Wilson plot yiel ed a value β_r for each of the swaged tubes equivalent to the theoretical value $\beta_s = 0.925$ (or the practically determined averaged value $\beta_s = 1.34$) for the smooth tube. This experimental value β_r can be compared to an appropriate theoretical value which can be derived for the swaged type of tube by an analysis

such as is outlined in the Appendix. This theoretical value β_r^*, appropriate to the constant in the Wilson plot, is

$$\beta_r^* = 0.925 \left(\frac{H - bN}{H}\right)\left(\frac{LN}{H}\right)^{1/3} \tag{12}$$

5.2 Pressure Drop Measurements

The friction factor f_r was calculated from the corrected pressure loss

$$\Delta P_r = 8\, f_r \cdot \frac{L}{D_h} \cdot \frac{V^2}{2g} \tag{13}$$

where V is the true axial velocity in the profiled section and D_h the true hydraulic diameter. Test runs with the smooth tube showed the expected relationship between f_s and the Reynolds Number $Re = \rho V D_s/\mu$. The smooth tube data were best represented by the Drew[11] equation plus 3% for the particular roughness of the commercial smooth brass and copper tubes used. Thus the fitted equation for the smooth tube is

$$f_s = 0.00072 + 0.0645\, Re^{-0.32} \tag{14}$$

Figure 11 shows typical plots, on logarithmic axes, of the profiled tube pressure drop ΔP_r against the water velocity V_s into the tube smooth end for a series of 4 start tubes of varying helix ratio. Note the increase of the slope of the lines from 1.78 to 2.02 as the helix ratio decreases. The slope of 2.02 indicates that the friction factor is independent of the Reynolds Number and, by analogy with smooth tube flow characteristics, that the flow is here fully turbulent.

Figure 12 shows typical plots of the profiled tube friction factor f_r against the Reynolds Number Re for the same tubes as are represented on Figure 11. These plots are extended to lower Re values as a result of isothermal experiments under cold flow, 70 F (21 ^{o}C), conditions. One can see by comparison of Figures 11 and 12 that the ratios $(\Delta P_r/\Delta P_s)$ are greater than the ratios (f_r/f_s). For example, for tube S.3 at a velocity V_s of 5 ft/sec the ratio $(\Delta P_r/\Delta P_s)$ is 4.25, while the equivalent ratio (f_r/f_s) is only about 3.3. This is because the pressure drop plots, Figure 11, include pressure losses due to the reduced cross sectional area for flow and reduced hydraulic diameter of the profiled tubes compared to the original smooth tube. The friction factors were computed using the true values V and D_H of the profiled tubes. Thus any increase of f_r over f_s is unequivocally due to the modification of the fluid flow characteristics by the profile shape, and analysis can proceed on this assumption.

6. Correlation and Interpretation of Results

The experimental data obtained is analysed in terms of the theoretical treatment outlined in section 4. The analyses are performed only for tubes of types (a), (b) and (c), the helically indented variety.

6.1 Heat Transfer Analysis - Water Side Results

The Swirl Flow model for predicting water side forced convective coefficients leads to equation (2)

$$\frac{\varepsilon_r}{\varepsilon_s} = \left(1 + \frac{1}{H_R^2}\right)^{.4} \qquad (2)$$

Values of ε_r have been experimentally determined, as outlined in section 5, and Figure 13 shows the ratio $(\varepsilon_r/\varepsilon_s)$ plotted against the quantity $(1 + 1/H_R^2)$ on log-log axes. Data for the 4 and 8 start swaged tubes, types (a), (b) and (c), are shown on this plot. The theoretical line at a slope of 0.4 is also drawn and one can see reasonable agreement between the experimental values $(\varepsilon_r/\varepsilon_s)$ and the theoretical prediction. Only in the case of the 4 start tubes S.21 and S.22 is there serious disagreement between theory and experimental measurement. These tubes have the shortest helix ratios, 0.210 and 0.280 respectively (see Table 1) of all the 4 and 8 start tubes in the series.

The Swirl Flow model assumes that the water flows along the helical path of the indentations. Clearly, however, as the helix ratio decreases the indentations become increasingly normal to the axis of the tube appearing more as a roughness to the fluid flowing, and there must come a point at which the flow tends to spill over the indentations rather than follow them. From the experimental data on Figure 13 it seems a plausible assumption that for values of helix ration H_R less than about 0.4, i.e. values of $(1 + 1/H_R^2)$ greater than about 7, the flow no longer follows the indentations, but substantially spills over them. Certainly the swirl flow model becomes inapplicable for predicting the forced convective heat transfer coefficient at helix ratios less than about 0.4 and, pending further evidence, this should be recognised as a limit. It is vital, therefore, at the outset to determine whether a tube shape has the characteristics of a swirl inducer or a roughness. Note that the data points for the 8 start tubes fall very near the theoretical line and show good agreement with theory. This indicates that the number of starts is of no consequence as long as the swirling mechanism is generated.

There seems also to be an effect, though a secondary one, due to the tube indentation. The theory takes no account of indentation, assuming that as long as the fluid swirls along the path of the indentation its size is immaterial. This effect may be seen on Figure 13 by reference to the data points for tubes S.43, S.44, S.3 and S.46, all of which have approximately the same helix ratio of about 0.65. The ratio $(\varepsilon_r/\varepsilon_s)$ increases from about 1.6 for tube S.43 to about 2.0 for tube S.46 while the indentation ratio increases by a factor of 4 from 0.027 to 0.114. The effect is brought out more clearly in Figure 15, which shows that only for the largest indentation, tube S.46, is the ratio $(\varepsilon_r/\varepsilon_s)$ significantly affected.

6.2 Pressure Drop Analysis - Water Side Results

The derivations of the Swirl Flow theory yield equation (4) for the friction factor correlation

$$\frac{f_r}{f_s} = \left(1 + \frac{1}{H_R^2}\right)^{1.38} \qquad (4)$$

Figure 14 shows the ratio (f_r/f_s) plotted against $(1 + 1/H_R^2)$. Values of the ordinate were read off from plots such as Figure 12 at a single value of Reynolds Number (Re) equal to 10^5, since it was found that Re itself was a parameter.

Even though restricted to one value of Re the agreement between theory and experiment is not very good. At values of abscissa less than about 2, $(H_R > 1)$, the experimental points are up to 15% less than the predicted values. As the helix ratio decreases further, the experimental points fall away to a greater extent from the theoretical line until, at the smallest values of H_R, i.e. largest abscissa values, the experimental points for tubes S.21 and S.22 indicate little relevance to the Swirl Flow model. This increasing divergence from the model with decreasing helix ratio H_R suggests the flow within the tube spills more and more over the indentations as H_R is reduced. With tubes S.21 and S.22 the flow is probably completely normal to the indentations with very little swirl component.

The results on Figure 14 also indicate a strong effect of indentation on the ratio (f_r/f_s), a factor absent from the theory, which contributes to the apparent spread of data points. The effect of indentation is shown on Figure 15 where the ratios (f_r/f_s) for tubes S.43, S.44, S.3, S.46 and S.9 are plotted against the indentation ratio δ. The plot shows, at this Re value of 10^5, that the ratio (f_r/f_s) is proportional to δ to the 0.45 power. The above five tubes all have helix ratios of about 0.65, see Table 1. The inclusion of tube S.9, 8 start, among the 4 start tubes indicates that there is no significant difference between 4 and 8 start tube geometry.

Further insight into the nature of this effect of indentation can be gained from considering the (f_r/f_s) ratios for the four tubes S 20, S.19, S.18 and S.46, as shown on Figure 16. These tubes each have an indentation ratio of 0.11, i.e. the deepest indentation of all the tubes tested. The data points lie on a straight line of slope near the theoretical one, and, for these tubes alone, the agreement with theory is much more reasonable than for all the tubes shown on Figure 14. A plausible assumption therefore is that the effect of indentation is simply one of directing the fluid flow into a more truly swirling path as the indentation increases.

6.3 Empirical Correlation of Pressure Drop Results

The experimental data thus shows that the ratio (f_r/f_s) is a function of the helix ratio H_R, the indentation ratio δ and the Reynolds Number Re. Therefore, from a purely practical viewpoint, an empirical equation relating (f_r/f_s) to these variables should be useful. The data points to be fitted by an empirical equation were gathered as follows.

From plots such as Figure 12 values of the ratio (f_r/f_s) were read for each tube at five parametric values of Re. These values were Re = 10^4, 3.10^4, 6.10^4, 10^5, 3.10^5 and imply a "smoothing" of the individual data points on the original plots of f_r vs Re. All the 8 start tubes were included in this process, and all the 4 start tubes with the exception of tubes S.21 and S.22. These two tubes were judged, from the previous analysis of heat transfer and pressure drop results, to have mechanisms quite different to the other 4 start tubes and so will be analysed separately.

Several forms of empirical expression were tested, the most successful being

$$\frac{f_r}{f_s} = 1 + 6.0647 \frac{\delta^x}{H_R^{1.815}} \qquad (15)$$

where the index x is a function of Re given by

$$x = 0.7384 - 0.1948 \cdot 10^{-6}(Re)$$

A test of the goodness of fit of equation (15) above can be seen on Figure 17 where the experimentally measured values of the ratio (f_r/f_s) are compared with the values predicted by equation (15). The "data points" for the different values of Re are identified by different symbols, though it should be remembered that these are smoothed data points as explained above. Figure 17 shows that the empirical expression embraces all but 4 of the 105 points within a spread of ± 14%, though the parametric effect of Re is still apparent. The results for tubes S.46 and S.17 show the greatest effect of Re. These tubes have the shortest helix ratio and indentation ratio, which combination gives rise to the largest values of (f_r/f_s).

A slightly more convenient form of equation which can be fitted is

$$\frac{f_r}{f_s} = 1 + 3.656 \frac{Re^{.03715}\ \delta^{0.6872}}{H_R^{1.815}} \qquad (16)$$

This empirical equation does not fit the data quite as well as equation (15) since now all but 10 of the 105 points are embraced within a spread of ± 14%.

Empirical equations (15) and (16) can therefore be applied within the following range of parameters:

Reynolds Number, Re,	10^4 to 3.10^5
Indentation Ratio, δ,	0.02 to 0.12
Helix Ratio, H_R,	0.4 to 3.0.

6.4 Heat Transfer Analysis - Condensing Side Results

The theoretical analysis outlined in section 4 indicates that, for the particular conditions of the assumed model, the swaged tubes could provide condensing side coefficients up to about three times that of a smooth tube. This follows if the same temperature driving force, ΔT_o, is maintained across the condensing films, for both smooth and swaged tube experiments. In practice this is almost impossible to arrange, and a test of the theoretical derivations is best achieved by comparing the experimentally determined constant β_r for each tube with the theoretical value β_r* given by equation (12).

Figures 18 and 19 show the results of such a comparison for the 4 and 8 start tubes respectively. The experimental values for the 4 start tubes form a curve when plotted against helix lead which is very similar to the theoretical one (equation (12)) shown dotted. At longer helix leads (> about 100 mm) agreement between theory and experiment is good. At the shortest helix leads of 1½ to 2 ins. (38 to 51 mm) the measured value β_r falls steeply as predicted by the theory, though not at the

predicted abscissa values. The reason for this disagreement is undoubtedly because of the flooding which is seen to occur in practice. At the low helix leads the drainage channels appear more normal to the vertical drainage direction and the surface tension forces are unable to prevent the condensate from spilling over the indentations. At these low helix leads therefore the condensate drains almost as on a smooth tube. The measured values β_r can be seen to be tending towards the measured value 1.3 for a smooth tube. The spread of some of the data points is inherent in the use of the Wilson plot for determination of β_r. The fuller interpretation of Figure 18 requires prediction of the onset of flooding on a vertically disposed tube of the "roped" variety.

The results on Figure 19 for the 8 start tubes show a maximum as predicted by the theory. However measured β_r values for the three tubes with helix leads greater than about 4 ins. (100 mm) are considerably higher than the theoretical prediction. A possible explanation for this could be that forces in addition to gravity are causing condensate drainage, while it is only gravitational forces which are considered by the theory. The 8 start tubes have twice as many drainage flats as the 4 start tubes, and hence thinner liquid films on them. These "flats" are slightly convex, and at the junction with the concave indentation surface tension forces could exist to cause drainage.

7. The Comparative Qualities of the Several Tube Types

As mentioned in section 2 detailed analysis of the heat transfer and pressure drop performance of the multifluted tubes, types (e) and (f), is beyond the scope of this paper. Yet their tube side and condensing side performance data, see Figures 8 and 10, show most interesting characteristics; the comparatively high condensing side coefficients being particularly worthy of note. The important question is to decide how, in economic terms, the different types of tube compare. The complete answer to this question can only be provided by comprehensive plant design studies, but a simple comparison can be made for the purposes of this paper as outlined below.

Ratios of the enhanced tube to smooth tube pressure drop ($\Delta P_r/\Delta P_s$), overall heat transfer coefficient (U_r/U_s), and tube side heat transfer coefficient (h_r/h_s) can be obtained for each of the enhanced tubes from plots such as Figures 4, 7 and 11. This has been done for each of the tubes in the 8 start helically indented series (type (c)), the multifluted tubes (types (e) and (f)) and a selection of the 4 start tubes (types (a) and (b)). The comparison has been made at one value of water flow into the tube smooth end, 5 ft/sec, so that all tubes being compared are handling the same mass flow of fluid. The numerical values are shown in Table 4.

Ideally one would look for a large value of the overall heat transfer coefficient ratio $(U_r/U_s) = \bar{U}$ and a comparatively small value of the pressure drop ratio $(\Delta P_r/\Delta P_s) = \bar{P}$. The ratio of these two quantities, defined as an Overall Performance Ratio (OPR) = $\bar{U}/\bar{P}$, is of significance, and one would be hoping for values in the region of 1. Another significant criterion is the Tube Side Performance Ratio (TPR) = $\bar{h}/\bar{P}$, where $\bar{h} = (h_r/h_s)$. Table 4 shows that the consistently largest values of OPR are obtained for the multifluted type of tube, these values being on average about 0.9. The 8 start (type (c)) and 4 start

helically indented tubing (types (a) and (b)) have average values of about 0.7 and 0.5 respectively. Note also that in most cases the TPR values are less than the OPR values. For this situation this implies that, of the total enhancement for a tube, a greater proportion is being obtained by the enhancement on the condensing side than on the tube side.

Table 4

Summary of Comparative Qualities of Tubes

All figures quoted assume water at 5 ft/sec (1.52 m/sec) flowing into tube smooth end

Tube Number	Tube Type	Pressure Drop Ratio $\bar{P} = \frac{\Delta P_r}{\Delta P_s}$	Overall Coefficient Ratio $\bar{U} = \frac{U_r}{U_s}$	Overall Performance Ratio (OPR) $= \frac{\bar{U}}{\bar{P}}$	Tube Side Coefficient Ratio $\bar{h} = \frac{h_r}{h_s}$	Tube Side Performance Ratio (TPR) $= \frac{\bar{h}}{\bar{P}}$
S.3	(a)	4.54	1.690	0.372	1.788	0.394
S.12	(a)	2.00	1.456	0.728	1.357	0.678
S.13	(a)	1.50	1.541	1.027	1.203	0.802
S.14	(a)	1.318	1.544	1.171	1.116	0.847
S.17	(a)	6.970	1.988	0.285	2.212	0.317
RM41	(b)	2.273	1.755	0.772	1.232	0.542
S.43	(a)	2.045	1.399	0.684	1.556	0.761
S.44	(a)	3.485	1.554	0.446	1.659	0.476
S.46	(a)	7.227	1.904	0.264	2.476	0.343
S.4	(c)	3.088	1.821	0.590	1.472	0.477
S.7	(c)	4.382	2.023	0.462	1.902	0.434
S.9	(c)	3.759	1.905	0.535	1.675	0.471
S.10	(c)	1.794	1.702	0.949	1.258	0.701
S.11	(c)	1.66	1.607	0.968	1.193	0.718
S.16	(c)	1.787	1.565	0.876	1.264	0.707
S.8	(d)	5.97	2.109	0.353	2.129	0.357
G.6	(e)	2.103	1.798	0.855	1.315	0.625
G.30	(e)	2.152	1.926	0.895	1.466	0.681
G.31	(e)	1.909	1.868	0.978	1.338	0.701
G.32	(e)	2.515	2.036	0.809	1.659	0.766
G.33	(e)	1.742	1.904	1.091	1.228	0.705
G.35	(f)	2.030	1.846	0.909	1.370	0.675
G.36	(f)	2.030	1.736	0.855	1.337	0.659
G.47	(f)	1.470	1.609	1.094	1.190	0.586

The above comparisons have been made under the very restricted range of parameters covered in these experiments and this must be borne in mind. But the main inference to be noted from Table 4 is that the multifluted type of tube is inherently capable, in this vertical orientation, and within the limits of the experiment, of providing overall enhancements equivalent to those of the helically swaged and indented tubing but with a smaller pressure drop penalty. Since manufacturing costs will not differ appreciably between these types of tubing the multifluted type, at least within the restricted field noted above, is to be preferred. The multifluted type of tube because of its longer lead construction achieves most of its total enhancement on the condensing side, practically free of energy loss penalty, with a much smaller enhancement (see Figures 8 and 10), and hence small pressure loss penalty, on the tube side. The helically swaged and indented

tubes, by contrast, obtain a larger proportion of their total enhancement on the tube side and this, of necessity, attracts a larger pressure drop penalty.

The data presented in this paper may be used to assess the performance of these enhanced tubes in the horizontal mode. Clearly, values of the inside coefficient will apply even if the tubes are in the horizontal mode. The condensing side coefficient can hardly be expected to show any increase over smooth tube values, however, since in a horizontal tube bundle the condensate drainage from one row of tubes to the next would destroy the delicate surface tension mechanisms responsible for enhancement. Yet, because horizontal drainage lengths are short, being only half a tube circumference, condensing side coefficients would be higher than for vertical smooth tubes. Therefore enhanced horizontal tubes could probably achieve overall coefficients as good as vertical multi-fluted tubes, say, whose major enhancement is on the condensing side. Enhanced condenser tubes in the horizontal mode therefore would derive all their enhancement from the increase in the tube side coefficient. For this reason horizontally disposed tubes would need to be of types (a), (b) or (c) and would therefore incur the comparatively high pressure drop penalty referred to above.

8. Discussion

The important inferences to be made from the foregoing studies relate to the use of the tubes in designs of advanced MSF plants or as preheaters in a ME train. The results of design studies utilising enhanced tubing in advanced MSF designs will be published at a later date, but this section discusses the various design philosophies which could embody enhanced condenser tubing.

There are previous published proposals[12,13] for utilising enhanced tubes in the horizontal mode in advanced MSF plants. Though details are scarce these tubes seem to be of the "roped" variety with helix ratios less than about 0.5. Here the enhanced performance of the tubes must stem almost completely from enhancement of the forced convective coefficient on the tube side, and this implies the pressure drop penalty referred to above. However in moving from a smooth tube to enhanced tube design there is scope for using a larger diameter enhanced tube, since, because of the increased heat transfer rate, the ratio of tube surface area to cross sectional area for flow can be reduced. By this means the enhanced tube design could have a pressure drop slightly less than the equivalent smooth tube design as well as achieve a saving in overall tube costs. When using enhanced condenser tubes to replace smooth ones there will usually be this opportunity to use a larger diameter tube and so avoid the pressure drop penalty.

Condenser tubes can also be used as vertically disposed bundles in MSF plants. Early designs, e.g. reference 14, employed vertical tube bundles for geometrical convenience with the small sizes of plant that were then being built. Subsequent larger plants, from 500,000 gal/d upwards, found the horizontal disposition more convenient. However even at sizes in the 5.10^6 gal/d range vertically disposed tubes can be used to advantage. Here the multifluted type of tube, types (e) and (f), is preferred to the other types. The tube profile produces such high condensing side coefficients that the main disadvantage of vertical tubes is circumvented. The pressure drop increase with this type of tube is generally less than for types (a), (b) and (c). In the opinion of the authors vertically

mounted tubes of the multifluted type would show greater advantages in MSF plant than horizontally mounted tubes of the "roped" type. For this vertical tube design some redisposition of the flash boxes can, with advantage, be employed. At the previous desalination conference in Dubrovnik, 1970, Tokmantsev et al.[15] described an MSF plant design using vertical enhanced tube bundles, though no details of tube shape were given.

The above comments also apply to the feed preheater stages of the ME system which are effectively elements of an MSF train. In addition small sizes of vapour compression ME plants, less than say 100,000 gal/day, could well use the multifluted type of tube, whether in upflow or downflow. The high condensing side coefficients are ideally suited to the evaporating side performance.

9. Conclusions

1. Several different types of profiled condenser tube shapes with enhanced heat transfer qualities have been described.

2. A theoretical analysis of the heat transfer and pressure drop performance of the forced convective flow on the tube side and of condensing steam side is presented. This analysis is limited, for this paper, to one of the basic shapes described. All tubes are considered to be vertically orientated.

3. The analysis shows that both tube side and condensing steam side coefficients should be increased by up to 2½ to 3 times smooth tube values under practical operating conditions.

4. Experiments at atmospheric conditions with 4 ft lengths of vertical profiled tubing showed that the tube side heat transfer performance was predicted fairly well by the analysis, the Swirl Flow Theory. The prediction of the tube side pressure drop was not so successful. Prediction of pressure drop is complicated by the effect of tube indentation which is not taken into account by the theory.

5. The simple theory for predicting condensing side heat transfer rates was only successful over a short range of the tube parameters. It is clear that complex phenomena such as condensate flooding over the indentations, and the influence of curved condensate surfaces upon drainage forces need to be considered.

6. Simple comparisons of the different tube types indicate that the multifluted type of tube should be superior to the other types for condenser duty in the vertical orientation.

Acknowledgements

The authors wish to acknowledge the expertise of Mr. H. Lloyd and Mr. M. Noakes, of Metallurgy Division, Harwell, in developing methods of profiled tube manufacture. They also wish to acknowledge the assistance of Mr. T. Hilton and Mr. D. Archibald who obtained the experimental results.

Bibliography

1. Oak Ridge National Laboratory, "Performance Characteristics of Advanced Evaporator Tubes for Long Tube Vertical Evaporators", O.S.W., Research and Development Progress Report No. 699, 1971.

2. Dukler, A. E. et al., "Experimental Program to Improve the VTE Distillation Process", O.S.W., Research and Development Progress Report No. 487, Sept. 1969.

3. Withers, J. G. and Young, E. H., Power Engineering, pp.44-45, June 1971.

4. Lawson, C. G., Kedl, R. J. and McDonald, R. E., Trans. Am. Nuc. Soc. 9, 565 (1966).

5. Wilson, E. E., Trans. Am. Soc. Mech. Eng. 37, 546 (1915).

6. Dittus, F. W. and Boelter, L. M. K., Univ. California (Berkeley) Publs. Eng. 2, 443 (1930).

7. Coulson, J. M. and Richardson, J. F., "Chemical Engineering" Vol. 1, pp.30 et. seq.

8. Nusselt, W., Z. Ver. deut. Ing. 60, 541 (1916).

9. Everett, M., Inst. Chem. Eng., The Chemical Engineer No. 231, 159 (1969).

10. Dukler, A. E., Am. Inst. Chem. Eng., Chem. Eng. Prog. Symposium Series, Storrs, 56, 1 (1960).

11. Drew, T. B., Koo, E. C. and McAdams, W. H., Trans. Am. Inst. Ch. E. 28, 56 (1932).

12. Burns and Roe Inc., "Use of Corrugated Tubes in Multistage Flash Evaporators", O.S.W., Research and Development Progress Report No. 731, October 1971.

13. Ebel, R. A. and Noritake, H. M., "The Value of Enhanced Heat Transfer Surface in a 150 mgd Multistage Flash Plant", O.S.W. Symposium on Enhanced Tubes for Distillation Plant, March 11-12, 1969, Washington D.C.

14. Franken, A., "Flash Evaporators for the Distillation of Sea Water", Proc. Inst. Mech. Eng., London 174, No. 7, p.312 (1960).

15. Tsimantsev, N. K. et al., 3rd International Symposium on "Fresh Water from the Sea", Dubrovnik 1970, Vol.4, pp.81-97.

16. Blasius, H., Forsch. Ver. deut. Ing. 131 (1913).

Nomenclature

A_i	Cross sectional area for flow inside tube
A_o, A_w	Surface area for heat transfer respectively of tube outer surface and at mean wall diameter
b	Width of grooves on outer surface of profiled tube
c	Specific heat of fluid flowing inside tube
D_s, D_h	Tube side hydraulic diameters of smooth and profiled tubes respectively
e	Depth of indentation on tube
f_s, f_r	Friction factors for smooth and profiled tubes respectively, see equations A.(8) and A.(10)
g	Gravitational acceleration
H	Helix lead, defined in section 2
H_R	Helix ratio, defined in section 2
h_i	Tube side heat transfer coefficient
h_s, h_r	Tube side coefficients for smooth and profiled tubes respectively
h_o, h'_o	Outside condensing coefficients for smooth and profiled tubes
k	Thermal conductivity of fluid
l	Reduced drainage length between indentations, see Figure 3
L	Total length of vertical tube
N	Number of starts or indentations round tube circumference
P_i, P_o	Inside and outside perimeters of profiled tube
Q	Heat transferred per unit area of surface
T_v, T_w	Temperature of condensing steam and tube outer surface respectively
U	Overall heat transfer coefficient
U_o	Overall heat transfer coefficient based on tube outer surface area
V_s, V	Average axial water velocity in smooth and profiled tubes respectively
x	Empirically derived index defined in equation (15)
β	Theoretical constant (= 0.925) in Nusselt equation, see equation (5)
β_r	Constant in Nusselt equation for profiled tubes derived from experimental data
β^*_r	Theoretically derived constant in Nusselt equation for profiled tubes, see equation (12)
γ	Tube performance ratio defined in section 4
ΔP	Pressure loss
ΔT_o	Temperature difference ($T_v - T_w$) across condensing film

ε_s, ε_r Constants in Dittus-Boelter equation (1) for smooth and profiled tubes respectively. Note that

$$h_r = \varepsilon_r \, Re^{0.8} \, Pr^{0.4} \, (k/D_h)$$

λ Latent heat of condensation of steam

ν Composite term defined by equation (10)

ρ Density of fluid

μ Viscosity of fluid

Re = Reynolds Number $\frac{\rho V D}{\mu}$

Pr = Prandtl Number $\frac{c\mu}{k}$

Appendix

Details of the derivation of the analyses for tube side heat transfer and pressure drop rates, and of condensing side heat transfer coefficient, are given in this appendix.

Tube Side Heat Transfer Analysis

As stated in section 4 the so called "Swirl Flow" model is used. The model assumes that the fluid flowing within the tube follows exactly the spiral path of the indentations (the criteria necessary to make the fluid swirl are not considered here). If the indentations lie at an angle θ to the axis of the tube (see Figure 3) of length L, then the actual swirling path length of the fluid at the wall will be $L/\cos\theta$. Because of this increased path length the swirl velocity at the wall is $V/\cos\theta$ where V is the axial velocity equal to the rate of fluid flow per unit of cross sectional area.

For flow in a smooth tube we have the well known Dittus-Boelter[6] equation for the tube side heat transfer coefficient h_s

$$\frac{h_s D_s}{k} = \varepsilon_s \left(\frac{\rho V_s D_s}{\mu}\right)^{0.8} Pr^{0.4} \qquad A.(1)$$

where the empirical constant ε_s has a value 0.023.

By analogy, in the swirl flow case we have

$$\frac{h_r D_h}{k} = \varepsilon_s \left(\frac{\rho V D_h}{\mu \cos\theta}\right)^{0.8} Pr^{0.4} \qquad A.(2)$$

or

$$\frac{h_r D_h}{k} = \varepsilon_r \left(\frac{\rho V D_h}{\mu}\right)^{0.8} Pr^{0.4} \qquad A.(3)$$

where subscripts r and s refer to profiled and smooth tubes respectively. Then assuming that the profiling does not appreciably change the hydraulic diameter and cross sectional area of the smooth tube, we have

$$\frac{h_r}{h_s} = \frac{1}{(\cos\theta)^{0.8}} = \frac{\varepsilon_r}{\varepsilon_s} \qquad A.(4)$$

But from Figure 3 one can see that the angle θ is related to the helix ratio H_R by

$$\cos^2\theta = \left(1 + \frac{1}{H_R^2}\right)^{-1}$$

Therefore

$$\frac{h_r}{h_s} = \left(1 + \frac{1}{H_R^2}\right)^{0.4} = \frac{\varepsilon_r}{\varepsilon_s} \qquad A.(5)$$

The derivation can be tested by plotting experimental values of $(\varepsilon_r/\varepsilon_s)$ against the quantity $(1 + 1/H_R^2)$ on log-log paper when a slope of 0.4 should be obtained.

Swirl Flow Model - Tube Side Pressure Drop Analysis

For flow in a smooth tube we have the pressure drop ΔP_s given by[7]

$$\Delta P_s = 8\, f_s \frac{L}{D_s} \frac{\rho V_s^2}{2g} \qquad \text{A.(6)}$$

By analogy for swirl flow in the profiled tube we have

$$\Delta P_r = C_f \frac{L}{\cos\theta\, D_h} \cdot \frac{\rho}{2g} \frac{V^2}{(\cos\theta)^2} \qquad \text{A.(7)}$$

where C_f is the coefficient of skin friction and is equivalent to $8\, f_s$ in a smooth tube.

Continuing the analogy we have by the Blasius[16] equation

$$f_s = 0.0396 \left(\frac{\rho V D_s}{\mu}\right)^{-0.25} \qquad \text{A.(8)}$$

and hence

$$C_f = 0.3164 \left(\frac{\rho V D_s}{\mu \cos\theta}\right)^{-0.25} \qquad \text{A.(9)}$$

$$\Delta P_r = \frac{f_s}{\cos\theta^{2.75}} \frac{L}{D_h} \frac{\rho V^2}{2g} = f_r \frac{L}{D_h} \frac{\rho V^2}{2g} \qquad \text{A.(10)}$$

$$\therefore \quad \frac{f_r}{f_s} = \frac{1}{(\cos\theta)^{2.75}} \qquad \text{A.(11)}$$

provided both smooth and profiled tubes have the same hydraulic diameter and cross sectional area.

Then, from the relationship between θ and H_R, we get

$$\frac{f_r}{f_s} = \left(1 + \frac{1}{H_R^2}\right)^{1.38} \qquad \text{A.(12)}$$

Analysis of Condensing Side Coefficient on Vertical Profiled Tubes

As explained in section 4 the analysis is restricted to profiled tubes of types (a), (b) and (c) where surface tension forces act to arrest drainage in the vertical direction. These forces effectively divide the total vertical length L of the profiled tube into short drainage lengths l between indentations as shown on Figure 3.

Following Nusselt[8] the average condensing coefficient h_o over a length L of vertical smooth tube with zero film thickness at the top is given by

$$h_o = 0.925 \left[\frac{\rho^2 g \lambda k^3}{\mu} \frac{A_o}{LQ}\right]^{1/3} \qquad \text{A.(13)}$$

$$h_o = 0.925 \left[K \frac{A_o}{LQ}\right]^{1/3}$$

where K represents the contribution of the physical properties of the condensed fluid.

Or, more conveniently for this analysis, since

$$Q = h_o A_o \Delta T_o,$$

where ΔT_o is the difference between saturated vapour temperature T_v and tube outer surface temperature T_w, then

$$h_o = 0.941 \left[K \frac{1}{L \Delta T_o} \right]^{\frac{1}{4}} \qquad \text{A.(14)}$$

Now applying this general equation A.(13) to any of the reduced drainage lengths l (see Figure 3) we have

$$h_o'' = 0.925 \left[K \frac{a_o}{lq} \right]^{1/3} \qquad \text{A.(15)}$$

where a_o and q refer to the surface area of, and heat transferred to, the single drainage strip of length l. The heat flux (q/a_o) in equation A.(16) is equivalent to Q'/A_c' where Q' is the total heat transferred over the entire enhanced tube length L, and A_o' is the total surface area of the tube outer surface minus the area of the indentations. Converting h_o'' to a coefficient h_o' based on the whole outer surface area A_o of the enhanced tube we have

$$h_o'' \left(\frac{l}{b + l} \right) = h_o' = 0.925 \left(\frac{l}{b + l} \right) \left[K \frac{A_o'}{lQ'} \right]^{1/3} \qquad \text{A.(16)}$$

Note, Q' for the enhanced tube case will be greater than Q.

Then since $Q' = h_o' A_o \Delta T_o$ equation A.(16) becomes

$$h_o' = 0.941 \left(\frac{l}{b + l} \right) \left[K \frac{1}{l \Delta T_o} \right]^{\frac{1}{4}} \qquad \text{A.(17)}$$

i.e.

$$h_o' = 0.941 \left(\frac{H - Nb}{H} \right) \left[K \frac{1}{l \Delta T_o} \right]^{\frac{1}{4}} \qquad \text{A.(18)}$$

Equation A.(18) expresses the condensing side coefficient h_o' for the enhanced tube. Comparing h_o' and h_o, the smooth tube coefficient, at the same temperature driving force conditions ΔT_o, we find

$$h_o' = h_o \left(\frac{H - Nb}{H} \right) \left(\frac{L}{l} \right)^{\frac{1}{4}}$$

i.e.

$$h_o' = h_o \left(\frac{H - Nb}{H} \right) \left(\frac{L}{(H/N) - b} \right)^{\frac{1}{4}} \qquad \text{A.(19)}$$

Equation A.(19) says that the enhanced tube coefficient will exceed the smooth tube coefficient (under the same temperature driving force conditions) by the enhancement factor EF, where

$$EF = \left(\frac{H - Nb}{H} \right) \left(\frac{L}{(H/N) - b} \right)^{\frac{1}{4}} \qquad \text{A.(20)}$$

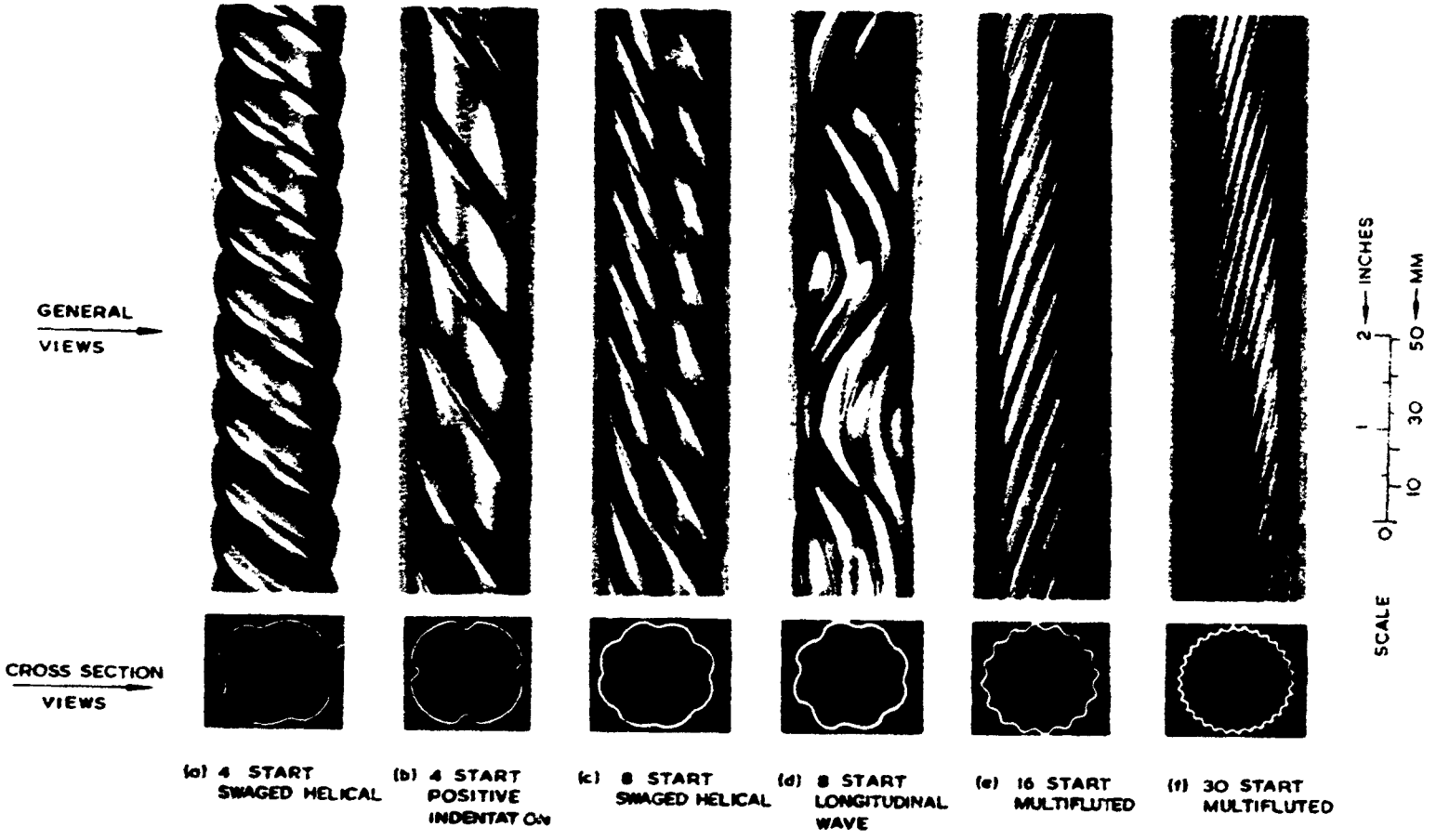

AERE - R 7318 Fig. 1
Views of different types of enhanced heat transfer tubing.

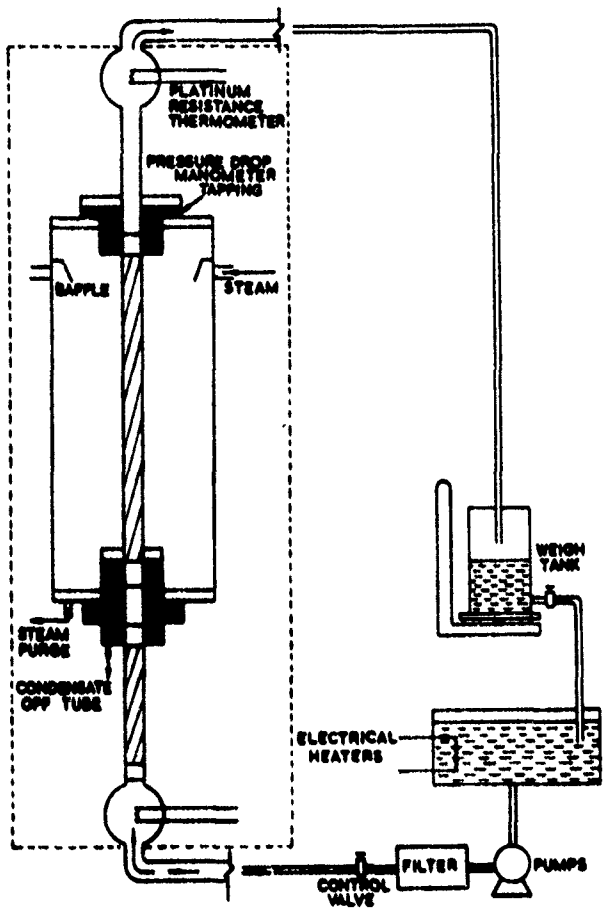

FIG. 2. SCHEMATIC REPRESENTATION OF HEAT TRANSFER APPARATUS
A.E.R.E. R.7318

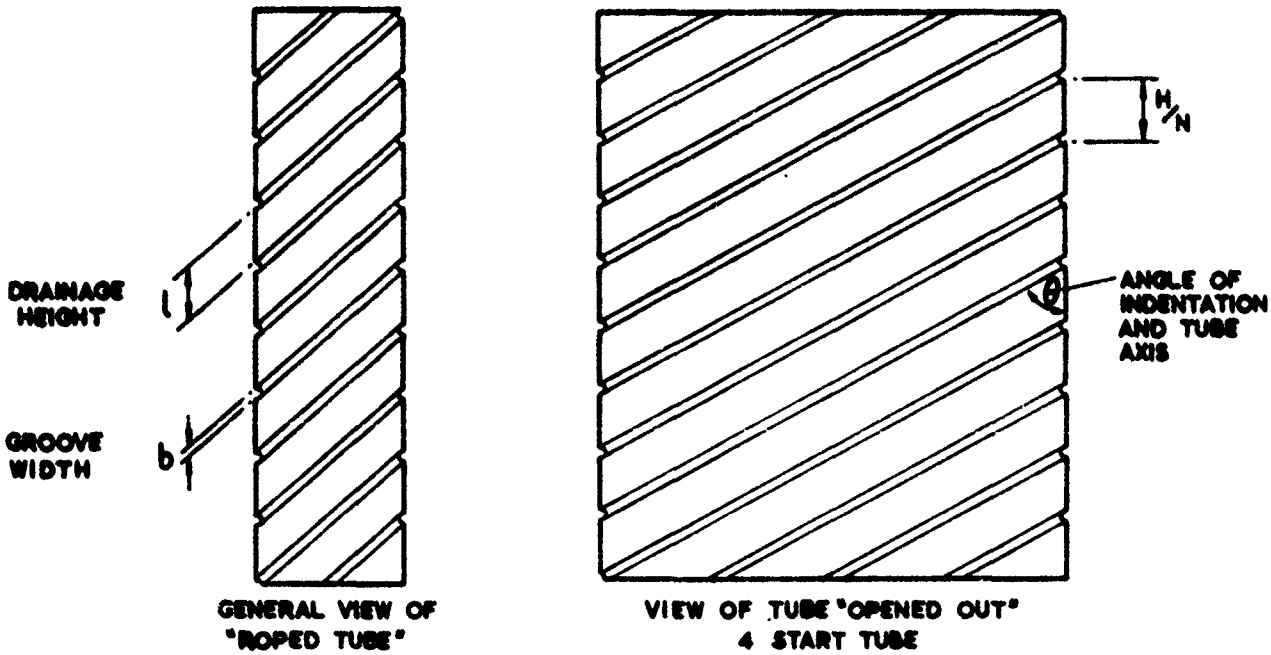

FIG. 3. MODEL FOR SWIRL FLOW THEORY AND FOR ANALYSIS OF CONDENSATION ON VERTICAL SWAGED TUBES.
A.E.R.E. R.7318

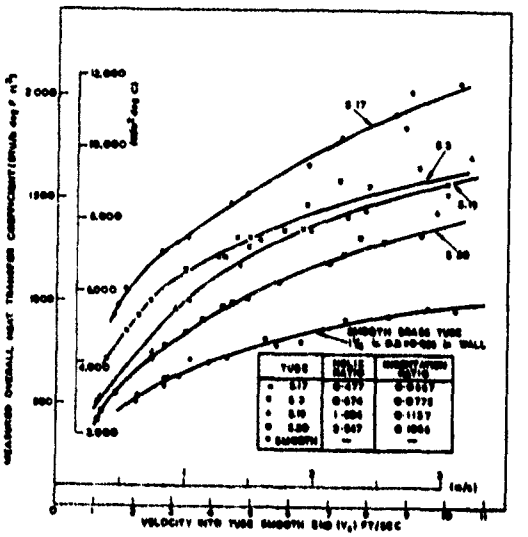

FIG 4 MEASURED OVERALL HEAT TRANSFER RATES - 6 STRAIGHT BRASS TUBES (TYPE B)
ASME 8.720

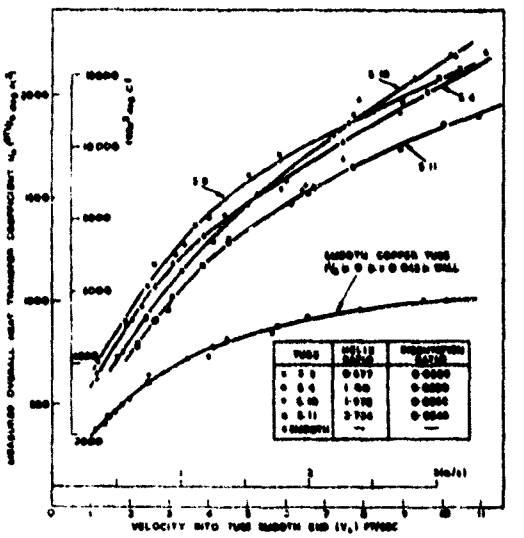

FIG 5 MEASURED OVERALL HEAT TRANSFER RATES - 6 STRAIGHT COPPER TUBES (TYPE C)
ASME 8.720

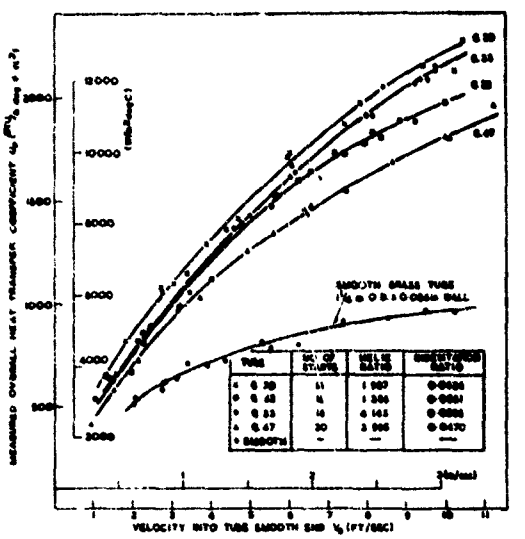

FIG 6 MEASURED OVERALL HEAT TRANSFER RATES - MULTIPLITED TUBES (TYPES B AND C)
ASME 8.720

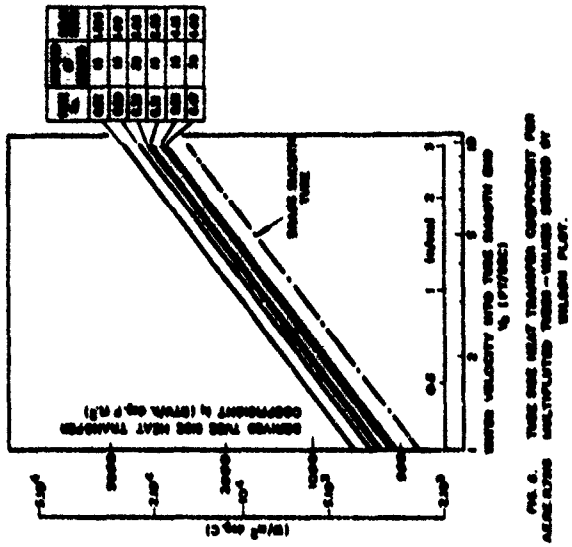

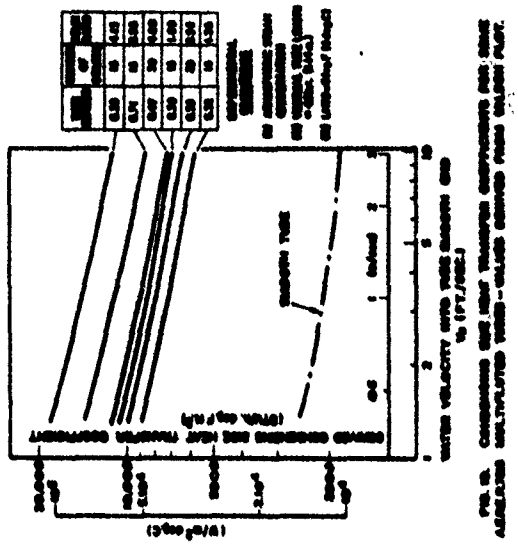

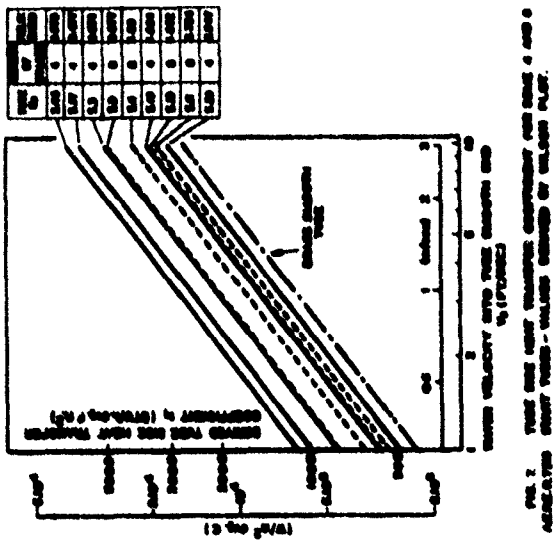

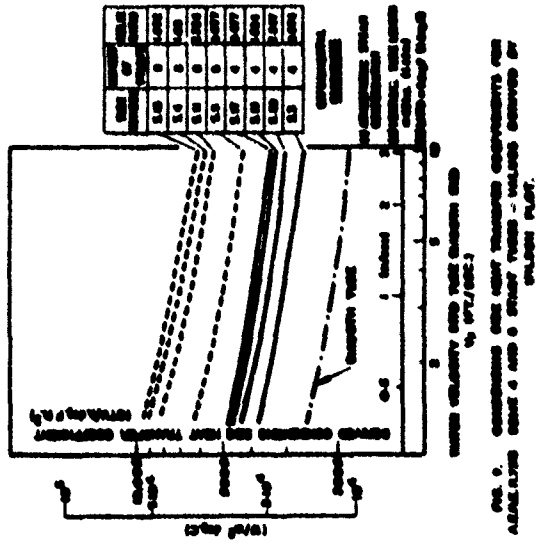

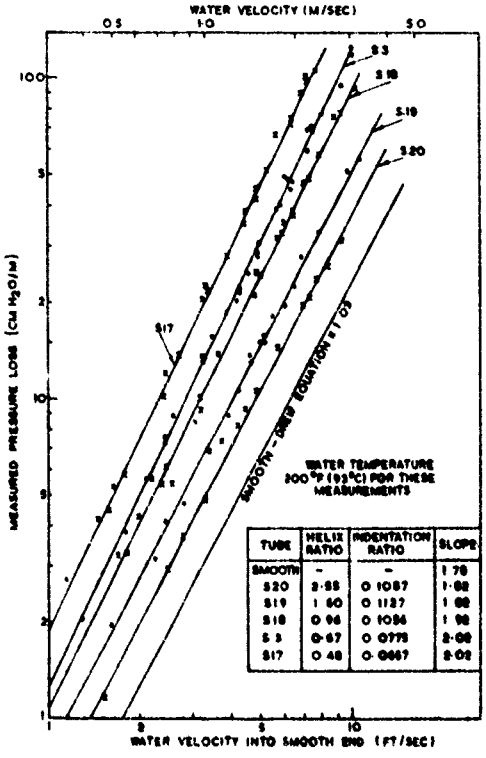

TUBE	HELIX RATIO	INDENTATION RATIO	SLOPE
SMOOTH	-	-	1·75
S.20	2·55	0·1087	1·82
S.19	1·60	0·1127	1·82
S.18	0·96	0·1056	1·98
S.3	0·67	0·0775	2·06
S.17	0·48	0·0667	2·02

FIG 11 CORRECTED PRESSURE DROP PER UNIT LENGTH
A.E.R.E. R.7316 vs VELOCITY INTO TUBE SMOOTH END

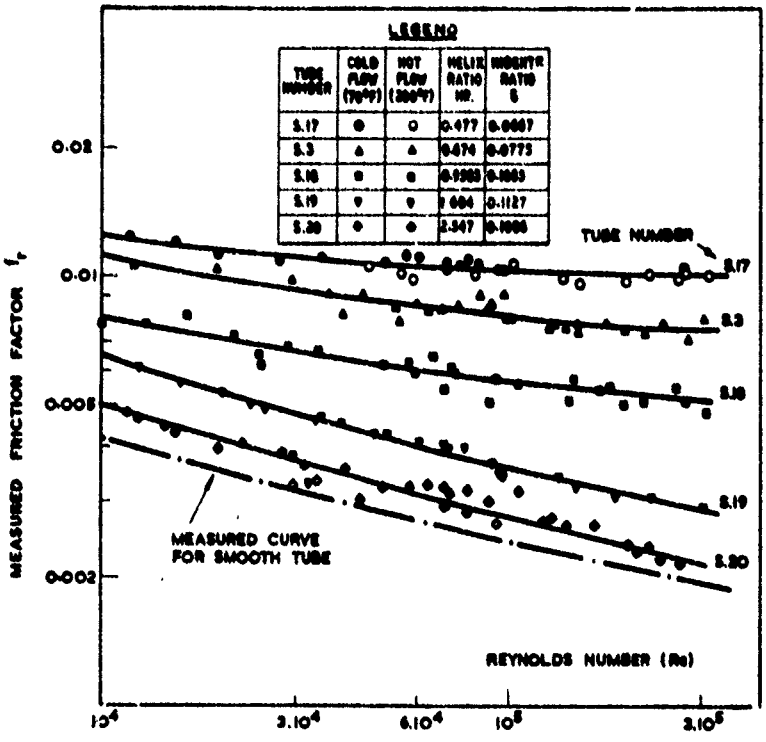

FIG. 12. TYPICAL FRICTION FACTOR PLOTS FOR 4 START TUBES SHOWN ON FIG. 13.
A.E.R.E. R.7316

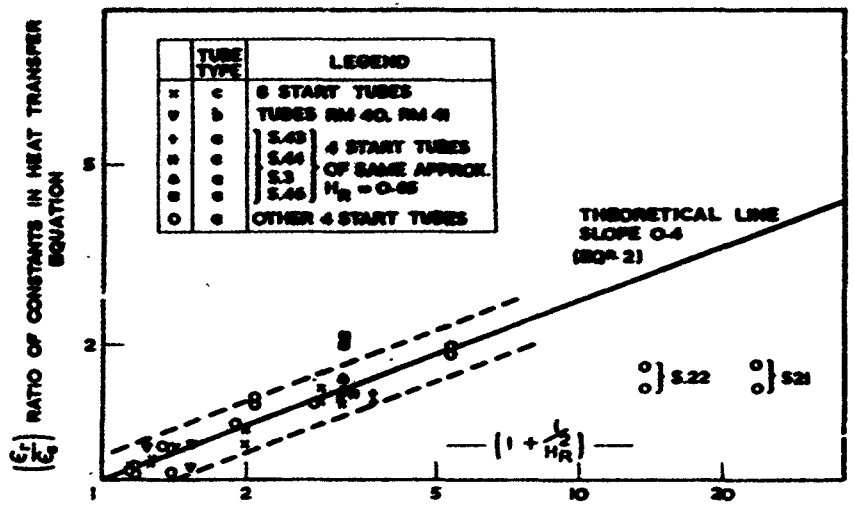

FIG. 13. A.E.R.E. R.7318 COMPARISON OF SWIRL FLOW THEORY HEAT TRANSFER PREDICTIONS WITH EXPERIMENTAL RESULTS.

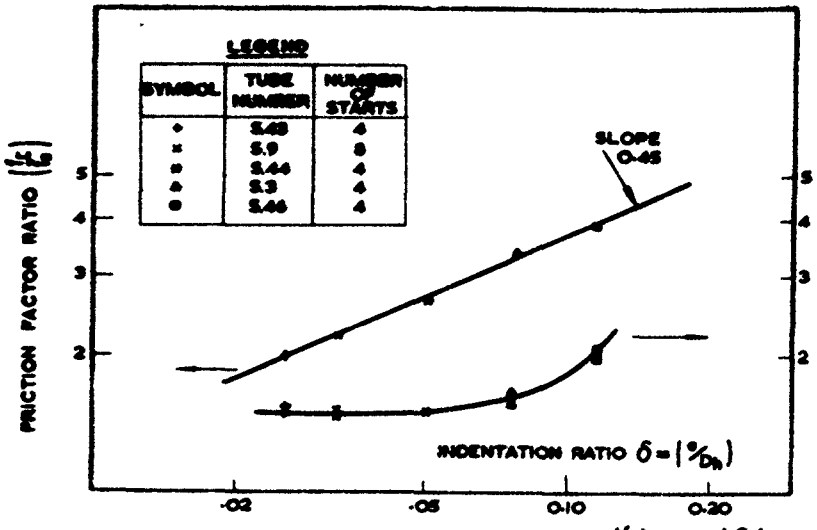

FIG. 15. A.E.R.E. R.7318 THE EFFECT OF INDENTATION RATIO δ ON $\left(\frac{f_r}{f_s}\right)$ AND $\left(\frac{\epsilon_r}{\epsilon_s}\right)$ (VALUES OF $\left(\frac{f_r}{f_s}\right)$ AT $Re = 10^5$)

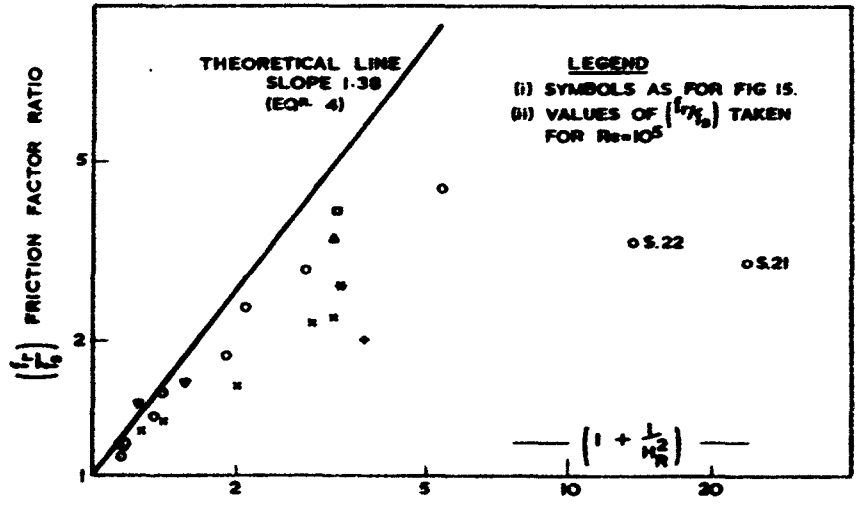

FIG. 14. A.E.R.E. R.7318 COMPARISON OF SWIRL FLOW THEORY FRICTION FACTOR PREDICTIONS WITH EXPERIMENTAL RESULTS.

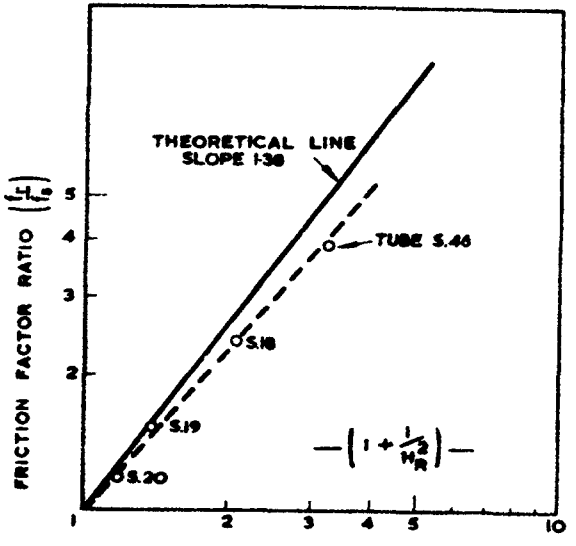

FIG. 16. A.E.R.E. R.7318 REPLOT OF DATA FOR TUBES WITH DEEPEST INDENTATION – DATA AT $Re = 10^5$ ONLY.

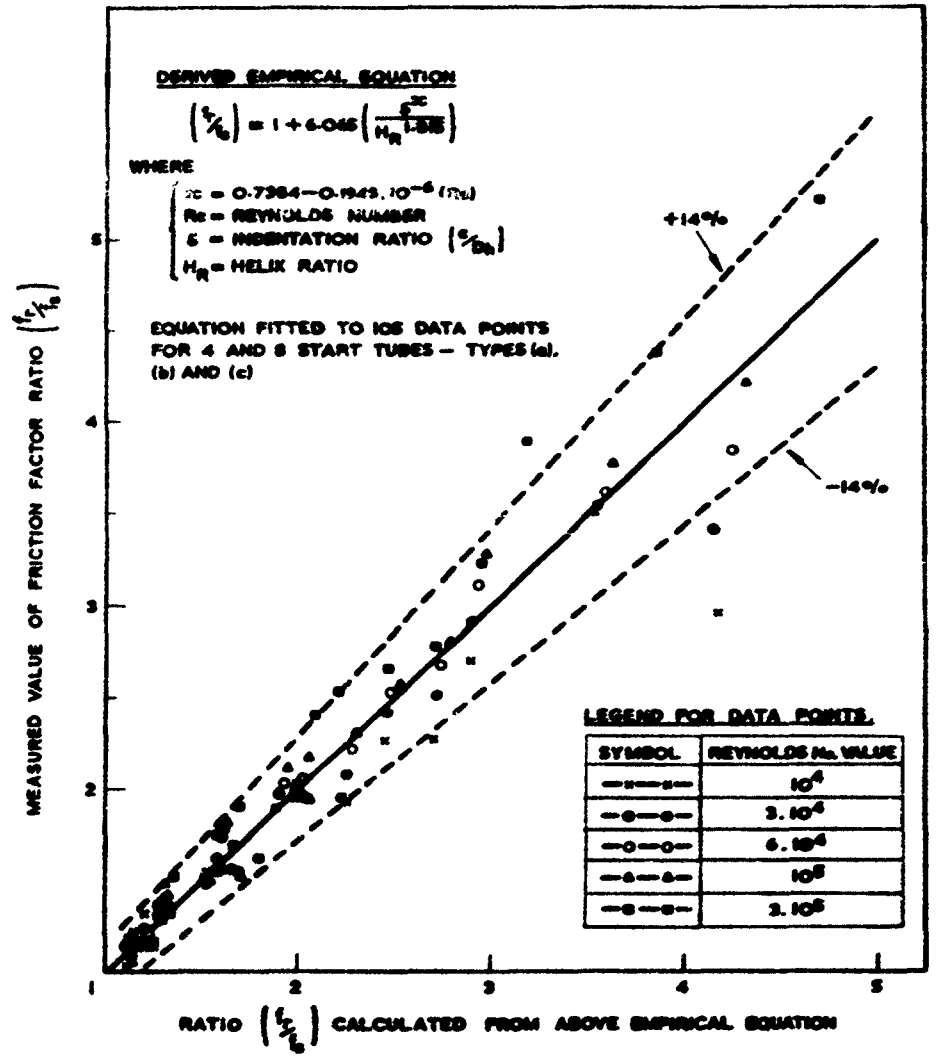

FIG. 17. TEST OF EMPIRICALLY DERIVED EQUATION FOR CORRELATING FRICTION FACTOR MEASUREMENTS.
A.E.R.E.R.7318

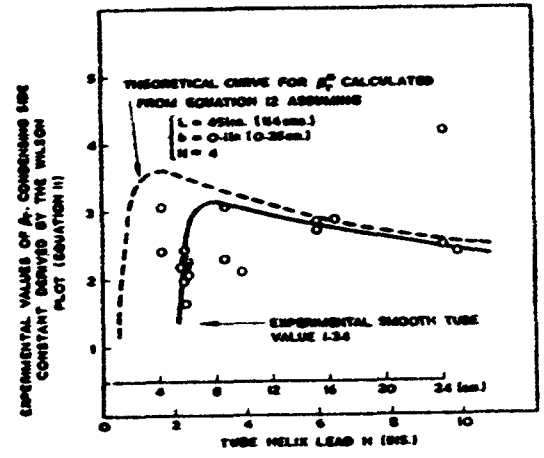

FIG 18. TEST OF CONDENSING SIDE HEAT TRANSFER COEFFICIENT ANALYSIS — MEASURED VALUES β_c FOR 4 START TUBES OF TYPE (a)
A.E.R.E.R.7318

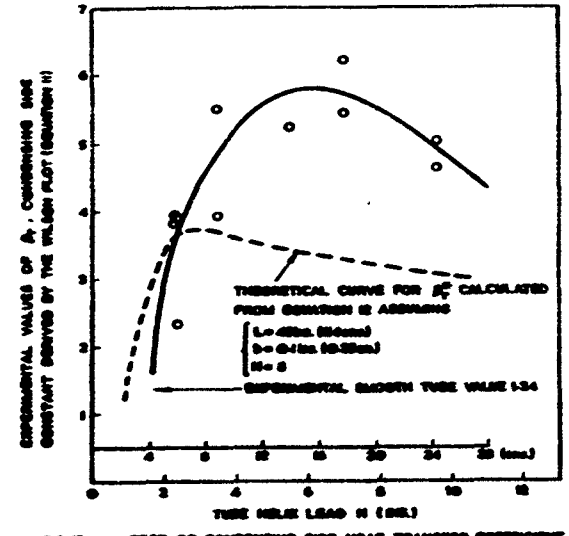

FIG 19. TEST OF CONDENSING SIDE HEAT TRANSFER COEFFICIENT ANALYSIS — MEASURED VALUES β_c FOR 8 START TUBES TYPE (d)
A.E.R.E.R.7318